International Tables for Crystallography (1983). Vol. A. Dordrecht: Kluwer.
ITO, T. & NOVACKI, W. (1974). *Z. Kristallogr.* **139**, 85-102.
KOCH, M. H. J. (1974). *Acta Cryst.* B**30**, 67-70.
KOJIĆ-PRODIĆ, B., RUŽIĆ-TOROŠ, Z., BRESCIANI-PAHOR, N. & RANDACCIO, L. (1980). *Acta Cryst.* B**36**, 1223-1225.
MAIN, P. & HULL, S. E. (1978). *Acta Cryst.* A**34**, 353-361.
NGUYEN-HUY DUNG, VO-VAN TIEN, BEHM, H. J. & BEURSKENS, P. T. (1987). *Acta Cryst.* C**43**, 2258-2260.
PATTABHI, V. & VENKATESAN, K. (1971). *Z. Kristallogr.* **134**, S81-90.
ROLLETT, J. S. (1970). In *Crystallographic Computing*, edited by F. R. AHMED. Copenhagen: Munksgaard.
SHI JIANQIU & SCHENK, H. (1988). *Proc. K. Ned. Akad. Wet. Ser B*, **91**, 237-244.
SCORDARI, F. & STASI, F. (1990*a*). *Neues Jahrb. Mineral. Abh.* **161**, 241-253.
SCORDARI, F. & STASI, F. (1990*b*). *Z. Kristallogr.* **190**, 47-62.
SHELDRICK, G. M. (1976). *SHELX*76. Program for crystal structure determination. Univ. of Cambridge, England.
SIM, G. A. (1961). In *Computing Methods and the Phase Problem in X-ray Analysis*, edited by J. ROLLETT. Oxford: Pergamon Press.
STEWART, J. M., MACHIN, P. A., DICKINSON, C. W., AMMON, H. L., HECK, H. & FLACK, H. D. (1976). The *XRAY* system - version of 1976. Tech. Rep. TR-446. Computer Science Center, Univ. of Maryland, College Park, Maryland, USA.
WATKIN, D. J. (1988). In *Crystallographic Computing* 4, edited by N. W. ISAACS & M. R. TAYLOR, pp. 111-125. Oxford Univ. Press.
WATKIN, D. J., CARRUTHERS, J. R. & BETTERIDGE, P. V. (1985). *CRYSTALS User Guide*. Chemical Crystallography Laboratory, Univ. of Oxford, England.

Acta Cryst. (1991). A**47**, 381-392

Crystal Lattices and Crystal Chemistry of Cylindrite and Franckeite

BY SU WANG

Beijing Laboratory of Electron Microscopy, Academia Sinica, PO Box 2724, 100080 *Beijing, People's Republic of China and China University of Geosciences at Beijing,* 100083 *Beijing, People's Republic of China*

AND K. H. KUO

Beijing Laboratory of Electron Microscopy, Academia Sinica, PO Box 2724, 100080 *Beijing, People's Republic of China and Laboratory of Atomic Imaging of Solids, Institute of Metal Research, Academia Sinica,* 110015 *Shengyang, People's Republic of China*

(*Received* 27 *April* 1990; *accepted* 17 *January* 1991)

Abstract

The crystal lattices and crystal structures of franckeite and cylindrite have been restudied using transmission electron microscopy. The selected-area diffraction, convergent-beam diffraction and high-resolution electron microscopy observations revealed that the relations between the two lattices and between the lattice and the structure modulation are various and incommensurate. Revised structure models of cylindrite and franckeite are proposed from the application of the structural principles found to form the basis of the crystal structure of angitorite for explanation of sinusoidal modulations in these minerals. The simulated and observed high-resolution electron microscopy images match very well. The crystallochemistry of cylindrite and franckeite is also discussed.

Introduction

The cylindrite group of minerals is important in crystallography because of their unique crystal structures with two interpenetrating types of layers which have different lattices. The reported cylindrite-group minerals include four species, cylindrite, franckeite, incaite and potosiite. Franckeite and cylindrite, originally described by Frenzel (1893) as samples from Bolivia and later discovered in many parts of the world, are the main minerals in this group.

Incaite and potosiite are very similar to franckeite in both structure and composition. Makovicky (1976) suggested that a small amount of Ag was essential to incaite and Kissin & Owens (1986) proposed that the substitution $Ag^{1+} + In^{3+} = 2Pb^{2+}$ exists in potosiite. Moh (1984, 1986), however, showed that small amounts of Ag were not essential to the synthesis of the cylindrite-group minerals and proposed that the so-called incaite was in fact franckeite with $Sn^{4+}:Sn^{2+} = 1$ and so-called potosiite was simply franckeite without Sn^{2+}.

The name cylindrite reflects the interesting morphological feature of this mineral to develop a cylindrical structure and cleavage. The mineral was previously studied by Moritz (1933) and Ramdohr (1960) in reflected light in polished section and by

0108-7673/91/040381-12$03.00

Makovicky (1971) using scanning electron microscopy. A detailed study of its structure using X-ray diffraction was performed later by Makovicky (1974, 1976), who suggested that this mineral possesses two interpenetrating lattices, a pseudo-tetragonal *A*-centered lattice and a pseudo-hexagonal *A*-centered lattice. Each of these lattices has a sublattice and a superlattice. He also suggested that the structure was composed of two kinds of layers corresponding to these two kinds of lattices. The layer with pseudo-tetragonal symmetry has composition PbS and is simply called the *t* layer; the layer with pseudo-hexagonal symmetry has composition SnS_2 and is called the *h* layer. These two kinds of layers are superimposed on each other forming a sequence *hththt*.... Each *t* layer is composed of two PbS layers which are similar to the PbS layer parallel to the (100) plane in the structure of galena. Each *h* layer is composed of two hexagonal close-packered layers of S atoms with most octahedral sites occupied by Sn, similar to the layers in the structure of berndtite. Makovicky (1976) also reported the lattice parameters: for the pseudo-tetragonal *A*-centered subcell $a = 11{\cdot}76$, $b = 5{\cdot}79$, $c = 5{\cdot}81$ Å, $\alpha = 90$, $\beta = 92{\cdot}38$, $\gamma = 93{\cdot}87°$; for the pseudo-hexagonal *A*-centered subcell $a = 11{\cdot}73$, $b = 3{\cdot}67$, $c = 6{\cdot}32$ Å, $\alpha = 90$, $\beta = 92{\cdot}58$, $\gamma = 90{\cdot}85°$; for the pseudo-tetragonal supercell $a = 140{\cdot}67$, $b = 5{\cdot}79$, $c = 75{\cdot}53$ Å, $\alpha = 90$, $\beta = 90{\cdot}01$, $\gamma = 93{\cdot}88°$; and for the pseudo-hexagonal supercell $a = 140{\cdot}37$, $b = 3{\cdot}67$, $c = 37{\cdot}92$ Å, $\alpha = 90$, $\beta = 90$, $\gamma = 90{\cdot}85°$. Makovicky also proposed that the superstructure period in the *c* direction was caused by the step-like corrugation of these layers.

Mozgova, Organova & Gorshkov (1976) studied the crystal structure of franckeite using X-ray diffraction and showed that its crystal structure, similar to that of cylindrite, also contained two kinds of layers. There are also two kinds of lattices corresponding to these two kinds of layers, the *t* lattice and the *h* lattice as in cylindrite. The main differences between the structures of franckeite and cylindrite are the thickness of the *t* layer and the long periodicity in these structures. He found that in the structure of franckeite the thickness of the *t* layer was twice that in cylindrite. Therefore, the *a* parameter (approximating the layer-stacking direction) of franckeite is greater than that of cylindrite. The sublattice parameters of franckeite given by Mozgova *et al.* (1976) were: $a = 17{\cdot}2$, $b = 5{\cdot}79$, $c = 5{\cdot}82$ Å for the *t* lattice and $a = 17{\cdot}2$, $b = 3{\cdot}65$, $c = 6{\cdot}3$ Å for the *h* lattice. Both of these lattices have long periods in both *c* and *b* directions. Mozgova *et al.* (1976) also reported that the long periods in the structure of franckeite were 8·148 nm in the *b* direction and 4·69 nm in the *c* direction.

Williams & Hyde (1988*a*, *b*) and Wang (1988, 1989) studied the crystal structure of cylindrite and franckeite using transmission electron microscopy (TEM). Contrary to the study of Mozgova *et al.* (1976), they did not observed the long period of 140 Å in the *a* direction in the structure of cylindrite and the 81·48 Å in the *b* direction in franckeite in their electron-diffraction patterns. Furthermore, they conclude from their HRTEM images that the long periodicity in the *c* direction in the structures of cylindrite and franckeite were caused by the sinusoidal modulation of the layers. Williams & Hyde (1988*a*, *b*) also simulated HRTEM images for cylindrite and franckeite with their wavy structure models and studied the electron-beam damage for franckeite with HRTEM images.

Though the structures of cylindrite and franckeite have been studied with HRTEM previously (Williams & Hyde, 1988*a*, *b*), several questions still remain. First, what is the relation between the two lattices of the structure? Second, how are the lattices related to the structure modulations in these minerals? Third, why do cylindrite and franckeite have wavy structure modulations? Fourth, what is the extent of beam damage in the electron microscope and what possible effects does this have on structural interpretation? We have restudied cylindrite and franckeite using transmission electron microscopy to try to answer these questions. Some of our SAED patterns and HRTEM observations are consistent with those of Williams & Hyde (1988*a*, *b*). The revised structure models of cylindrite and franckeite are suggested, simulated and discussed.

Samples and experimental details

The cylindrite sample used in this study came from the Geological Museum of the China University of Geosciences at Beijing. The provenance of this cylindrite sample is Poopo in Bolivia, the same place as that of the sample studied by Makovicky (1971, 1974, 1976). Morphologically, the cylinder axis is approximately along the [001] direction with the radius close to the [100] direction. This mineral has perfect {100} cleavage. The geological and mineralogical details have been described in previous works (Frenzel, 1893; Makovicky 1971, 1974, 1976; Mozgova, Borodayev & Sveshnikova, 1975). The franckeite sample used in this study occurs in fractures in the marls and megalenticular limestone on the outer flank of the upper veined-type tin ore bodies in Changpo ore deposit, Guangxi, China. The crystal habits are thin tabular {100}, striated [001] on the cleavage plane, usually massive or foliate. Crystals are often warped or bent with perfect {100} cleavages. The geological features have been thoroughly described by Huang, Wu, Chen & Tang (1986). The results of electron-microprobe analyses of the samples of cylindrite and franckeite are listed in Tables 1 and 2, respectively.

Thin specimens were prepared for TEM observations. Specimens parallel to the {100} cleavage plane

Table 1. *The chemical composition of cylindrite* (wt%)

Sample	Sn	Sb	Pb	S	Fe	As	Zn	Total
1	24·15	12·42	36·02	23·65	2·77	0·00	0·60	99·06
2	24·94	12·22	35·33	23·48	2·56	0·23	0·00	98·76
3	24·73	12·69	36·67	23·47	2·56	0·11	0·10	100·33
4	27·61	12·07	35·92	23·80	2·52	0·16	0·00	102·21
Mean	25·36	12·33	35·99	23·60	2·60			99·88

Table 2. *The chemical composition of franckeite* (wt%)

Sample	Pb	S	Sn	Sb	Fe	As	Total
1	55·59	20·22	10·96	11·38	1·86	0·00	100·01
2	55·70	20·27	10·98	11·84	1·86	0·00	100·65
3	55·45	19·81	11·63	10·84	1·98	0·30	100·01
Mean	55·58	20·10	11·19	11·35	1·90	0·10	100·22

were prepared by repeated cleavage between two pieces of cellophane tape. The method has been described in detail by Hirsch, Howie, Nicholson, Pashley & Whelan (1977). In order to get the cross-sectional thin specimens oriented normal to the {100} cleavage plane, cleavage slabs of 1 mm thickness were glued together between two silicon wafers with Epon 812 epoxy resin to form a sandwich. These sandwiches were fastened together and then ground and polished down to 30 μm thickness with its normal parallel or perpendicular to the cylinder axis in the case of cylindrite or to the striae on the cleavage plane in the case of franckeite. These sections were then ion thinned using a Gatan 600B ion mill. In order to minimize the damage in the process of ion milling a cooled stage was used. Philips EM 420 and JEOL-JEM 200CX electron microscopes were used in this study. Image simulations were done with a multislice program.

Electron-diffraction observation

The fundamental lattices of cylindrite and franckeite have been solved by previous X-ray and electron-diffraction studies. However, our TEM studies provide some detailed information about these structures and lattices. The main difficulty of studying these structures with the single-crystal X-ray diffraction method is to find good single crystals of these minerals. Owing to the curved nature of cylindrite and the aggregate nature of franckeite as well as their plasticity behaviour, good single-crystal X-ray diffraction patterns can rarely be obtained. In an electron microscope, one can easily obtain single-crystal electron diffraction patterns and high-resolution images of an area less than 1 μm to study the structure details in both reciprocal and real spaces. However, it is necessary to prepare proper thin-crystal specimens without severe mechanical and electron-beam damage, as described below.

Cylindrite

Fig. 1 presents the b^*c^* selected-area electron diffraction (SAED) patterns of the t lattice and the h lattice (the electron beam is approximately normal to the cleavage plane). Previous studies showed only the composite SAED pattern containing both lattices (Makovicky, 1976; Williams & Hyde, 1988*a*, *b*). We have successfully produced separate SAED patterns for each lattice by tilting the specimen slightly. The SAED patterns (Fig. 1) show that each main reflection is accompanied by a row of satellites indicated by the vector **q**. In most cylindrite crystallites, the direction of **q** is not parallel to the c^* axis defined by the main reflections. The angle between $\mathbf{c}^*$ and **q** projected on the b^*c^* plane varies from 0 to 6° for the h lattice and from 0 to 4° for the t lattice. Fig. 2 shows that **q** can either be parallel to (Fig. 2*a*) or make a small angle with the c^* axis of the t lattice (Fig. 2*b*). In the former case, the c^* of the h lattice and t lattice as well as **q** are all parallel to each other when projected on the b^*c^* plane and the long period indicated by the satellite spots is a common multiple of c of both lattices. This observation was mentioned previously by Makovicky (1974, 1976). The indices of

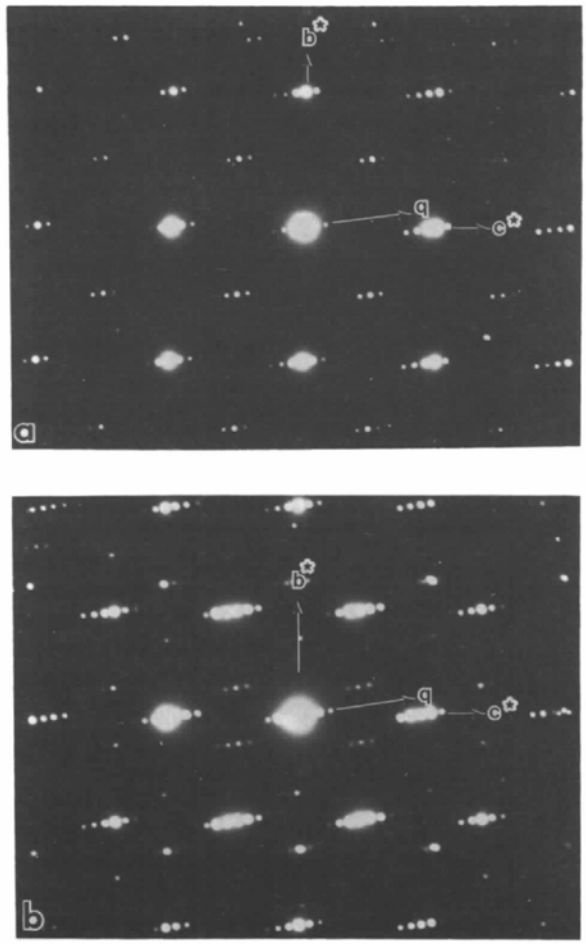

Fig. 1. b^*c^* plane SAED patterns of cylindrite. (*a*) t lattice; (*b*) h lattice.

satellites are rational. In the latter case, the basic axes (b and c) of these lattices are not parallel to each other in either real or reciprocal space and the indices of these satellites involve irrational numbers. As pointed out by Janner & Janssen (1980), irrational satellite indices are the result of an incommensurately modulated structure, whereas rational satellite indices indicate a superstructure. As we have seen above, the indices of these satellites could change from rational to irrational. The long periodicity, therefore, would be superstructure periodicity in some cases and incommensurate modulation periodicity in other cases. The indices of the satellites in the SAED pattern of cylindrite do not remain constant. In the case of γ-Na_2CO_3, the indices of satellites change continuously with temperature (van Aalst, den Hollander, Peterse & de Wolff, 1976). But the factors that influence the change of these satellite indices in the structure of cylindrite are still unknown.

Convergent-beam electron diffraction (CBED) patterns are very useful to determine the orientation relationship between the two lattices in three-dimensional space. Fig. 3 is an example showing such a relation. Figs. 3(a) and (b) are the [100] zone-axis CBED patterns of the cylindrite h lattice and t lattice, respectively, and Fig. 3(c) is a composite showing the relation between the two [100] zone axes. The differences in the zone axes are 4·5° for γ and 0·4° for β.

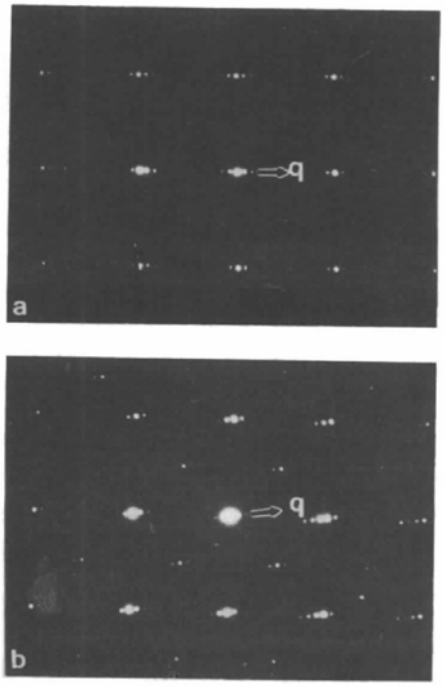

Fig. 2. b^*c^* plane SAED patterns of the t lattice of cylindrite showing the variance of **q**. (a) **q** is parallel to $\mathbf{c}^*$ on the projection of the b^*c^* plane. (b) **q** is not parallel to $\mathbf{c}^*$ on the projection of the b^*c^* plane.

Figs. 4 and 5 are the SAED patterns and schematic illustrations of the a^*c^* and a^*b^* planes of cylindrite, respectively, and are consistent with the observations of Williams & Hyde (1988a, b). The relation between the two lattices observed from CBED patterns is confirmed by the SAED pattern shown here.

From the SAED patterns shown in Figs. 1, 4 and 5, we can see that there are two different kinds of incommensurability in the structure. One is the incommensurability between the long-periodicity modulation and the basic lattices. Another is the incommensurability between the two sublattices described by Makovicky (1974, 1976). An incommensurate modulated crystal, such as cylindrite, does not have a three-dimensional lattice peridocity (Janner & Janssen 1980). The two basic lattices can be obtained from the main reflections. The resultant lattice parameters correspond to the subcells

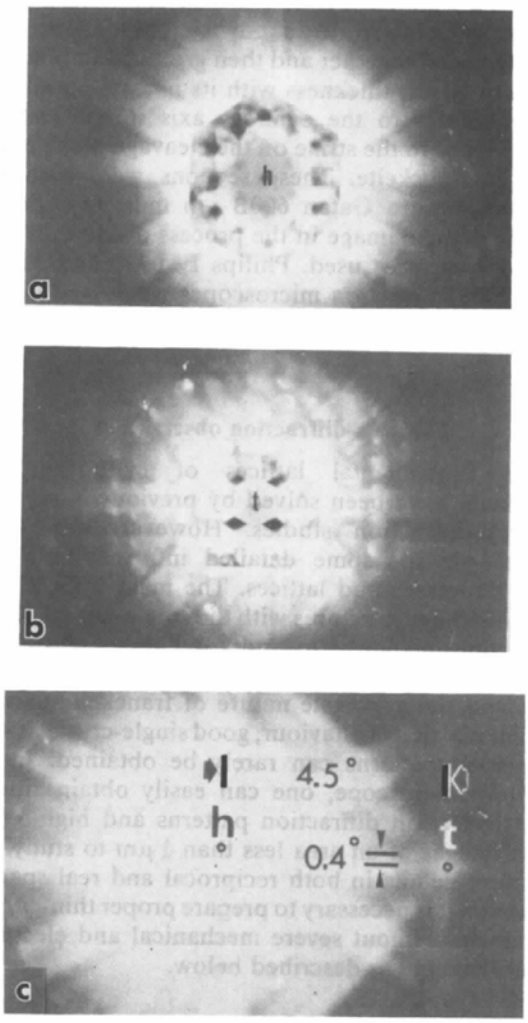

Fig. 3. [100] zone axes CBED patterns of cylindrite. (a) h lattice; (b) t lattice; (c) the pattern containing both the h lattice and the t lattice shows the relation between the two lattices.

described by Makovicky (1974, 1976). However, the angles between the axes we measured and those of Makovicky (1976, 1974) are somewhat different. The angles given by the SAED patterns in the present paper are: $\alpha = 91\,(2)$, $\beta = 92\,(1)$, $\gamma = 95\,(5)°$ for the t lattice; $\alpha = 91\,(3)$, $\beta = 91\,(6)$, $\gamma = 91\,(4)°$ for the h lattice. The common modulation wavelength for both lattices is 38 Å.

The symmetry of cylindrite, as an incommensurate modulated structure, cannot be described by a three-dimensional space group. However, it is possible, as de Wolff (1974, 1977) and Janner & Janssen (1977, 1980) have shown, to recover its space-group symmetry by constructing a periodic structure in a suitably defined four-dimensional space such that the crystal appears as a three-dimensional section. Usually, the extra basis vector **q** which is used to indicate the long-range modulation is described as follows:

$$\mathbf{q} = q_1\mathbf{a}^* + q_2\mathbf{b}^* + q_3\mathbf{c}^*.$$

A fourth index m is introduced in an extended form of the diffraction vector equation:

$$\mathbf{H} = h\mathbf{a}^* + k\mathbf{b}^* + l\mathbf{c}^* + m\mathbf{q},$$

where h, k, l and m are integers. The symmetry of the structure using superspace-group theory is described elsewhere (Wang, in preparation).

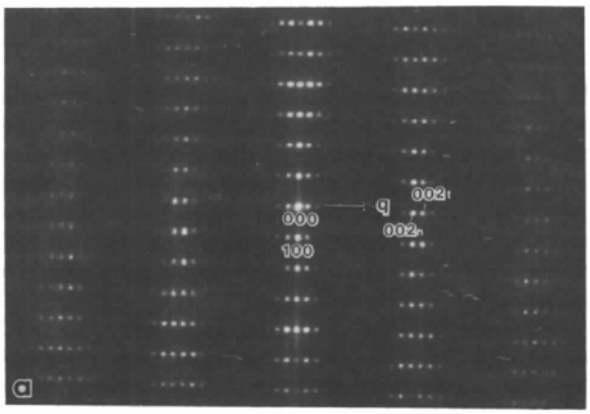

(*a*)

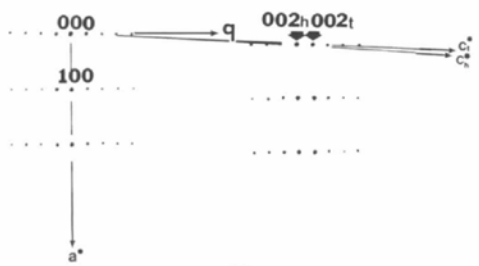

(*b*)

Fig. 4. a^*c^* plane SAED pattern of cylindrite (*a*) and its schematic illustration (*b*).

To determine the possible extent of radiation damage, the sample was subjected to a focused electron beam and SAED patterns of the area were recorded at regular intervals. When the electron beam is perpendicular to the layers, the sample is very resistant to damage. When the electron beam is parallel to the layers, the sample is damaged easily. The SAED patterns in Fig. 6 show that the h lattice becomes somewhat twinned at first (Fig. 6*b*) and severely twinned for longer irradiation (Fig. 6*c*); then the stacking repeat is doubled, as observed previously by Williams & Hyde (1988*a*, *b*); later, the 11·7 Å stacking repeat of the h lattice gradually disappears (Fig. 6*d*); finally, the crystal becomes amorphous. Nevertheless, the time that the crystal remains intact is long enough to allow one to take a HRTEM image and to make a SAED analysis.

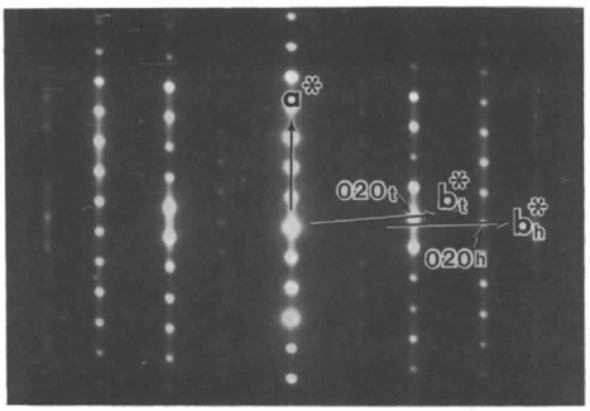

Fig. 5. a^*b^* plane SAED pattern of cylindrite.

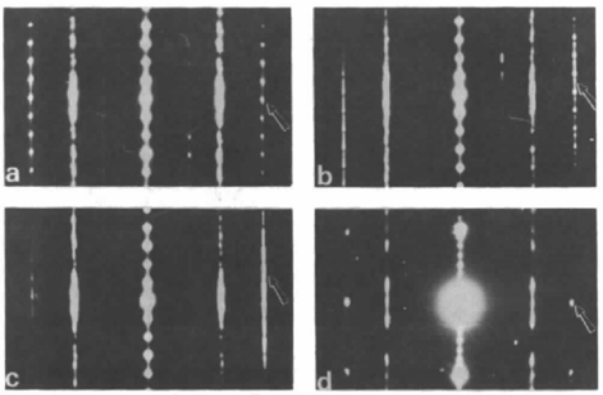

Fig. 6. A series of SAED patterns recorded for the same area of a cylindrite sample at regular intervals of time showing radiation damage. (*a*) First 15 min showing the original twinned t lattice sample. (*b*) Second 15 min showing the pattern becoming the twinned h lattice. (*c*) Third 15 min showing the h lattice becoming severely twinned. (*d*) Fourth 15 min showing that the stacking repeat has doubled and the h lattice has disappeared.

Franckeite

The structure of franckeite is similar to that of cylindrite. The SAED patterns of b^*c^*, a^*c^* and a^*b^* planes (Fig. 7) show that the basic b^*c^* meshes of the h lattices and the t lattices of both cylindrite and franckeite are similar in two respects: first, each main reflection is accompanied by a row of satellites whose direction is indicated by the vector **q**; second, the basic parameters defined by the main reflections are similar. In reciprocal space, the angle between the b^*c^* planes of the h lattice and the t lattice is so small that the separate b^*c^* SAED patterns of each lattice could not be observed. All b^*c^* SAED patterns for franckeite contain both lattices. There are also two kinds of incommensurability in the structure of franckeite. The incommensurability between the two lattices is apparent in all four patterns shown in Fig. 7. In spite of the fact that the c^* axis of both lattices is almost parallel to the vector **q** in the b^*c^* SAED pattern, the small angle between them is clear in Fig. 7(d). As shown in Fig. 8, **q** is not parallel to any axis in the (100) HRTEM image. Therefore, the relation between the long periodicity and the basic lattices is also incommensurate.

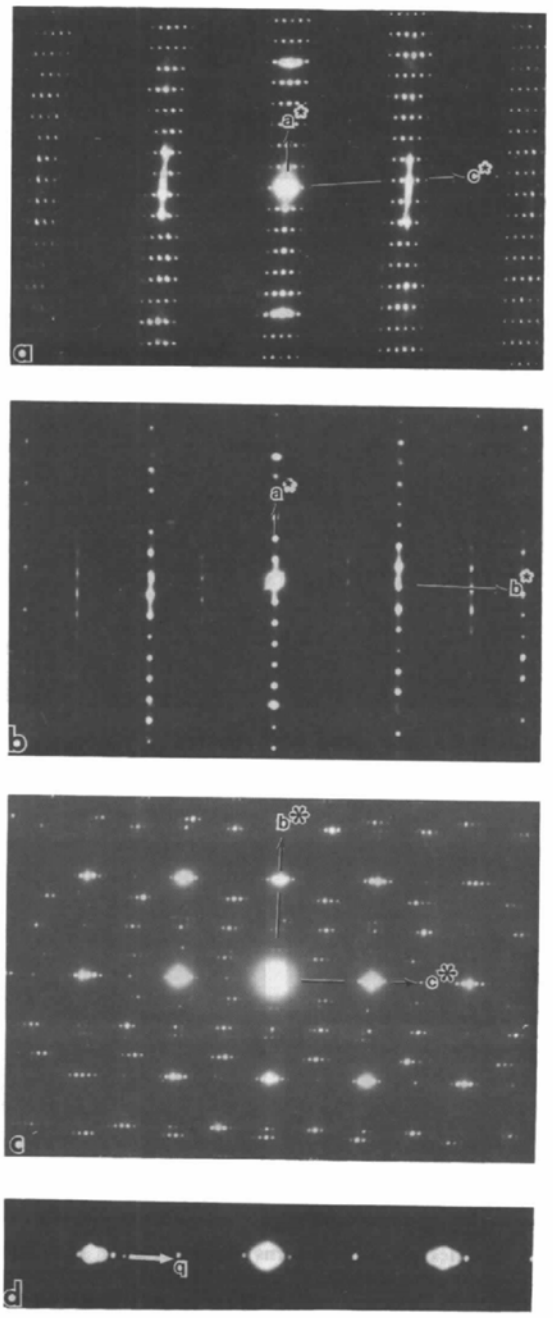

Fig. 7. SAED patterns of franckeite. (a) a^*c^* plane; (b) a^*b^* plane; (c) b^*c^* plane; (d) enlarged central part of b^*c^* plane showing **q** is not parallel to **c*** defined by main reflections.

The differences between the lattices of franckeite and cylindrite are clear. First, the two minerals have different layer repeats [$d_{(100)} = 11{\cdot}7$ Å for cylindrite; $d_{(100)} = 17{\cdot}3$ Å for franckeite]; second, the t lattice of franckeite is a primitive lattice while that of cylindrite is A centered; third, they have different wavelength of modulation (38 Å for cylindrite; 47 Å for franckeite).

The angles between axes given by the SAED patterns in this paper are somewhat different from previous values. They are $\alpha = 91\,(3)$, $\beta = 96\,(2)$, $\gamma = 88\,(6)°$ for the A-centered h lattice; $\alpha = 91\,(4)$, $\beta = 95\,(5)$, $\gamma = 88\,(2)°$ for the primitive t lattice.

HRTEM observation

As mentioned earlier, it is very difficult to study the details of the structure of cylindrite and franckeite because of the poor quality of single crystals. Furthermore, there are no proper methods or programs to resolve the structures which have two kinds of lattices and the two incommensurabilities mentioned previously. Electron microscopy is much more effective for studying these structures.

Fig. 9 presents the (100) HRTEM images of the h lattice and the t lattice of cylindrite. The image of the t lattice corresponds to the (100) simulated image of galena (PbS) shown in Fig. 10(a). Similarly, the image of the h lattice resembles the (100) simulated image of berndtite (SnS_2) shown in Fig. 10(b). These simulated images were determined without considering the effects of modulation and intergrowth. The assumption (Makovicky, 1974) that the structure of cylindrite is composed of a pseudohexagonal layer with a composition MeS_2 which essentially represents an octahedral SnS_2 layer and a pseudotetragonal layer which has the bulk composition MeS and represents a deformed galena-type structure is structurally confirmed by the separate h layer and t layer HRTEM images. Both layers have a common modulation which can be seen in Fig. 9 as dark bands. Obviously, the b and c axes of the h layer and the t layer are

not parallel to each other and the modulation vector **q** is not parallel to any axis.

The (010) HRTEM image of cylindrite (Fig. 11*a*) is consistent with the observations of Williams & Hyde (1988*a*, *b*). The sinusoidal modulation is the origin of the dark band in the image of the (100) plane in Fig. 9. The simulated HRTEM image based on the structure model revised from that suggested by Makovicky (1974) coincides well with the observed HRTEM image as shown in Fig. 11(*b*). The simulated image also shows this feature. Compared with the structure model given in Fig. 12, we can see that the brighter spots and lines in the image represent the vacancy between the *h* layer and the *t* layer; the weak spots and lines correspond to the vacancy in the *t* layer. The (001) HRTEM image (Fig. 13) also shows the same contrast, but without sinusoidal modulation.

The (100) HRTEM image of franckeite shown in Fig. 8 contains both the *h* layer and the *t* layer. Because of the curvature of this plane, hexagonal lattices appear in some areas and tetragonal lattices are evident in others. The image is complementary to the corresponding SAED pattern (Fig. 7*d*); together they show the exact relation between the

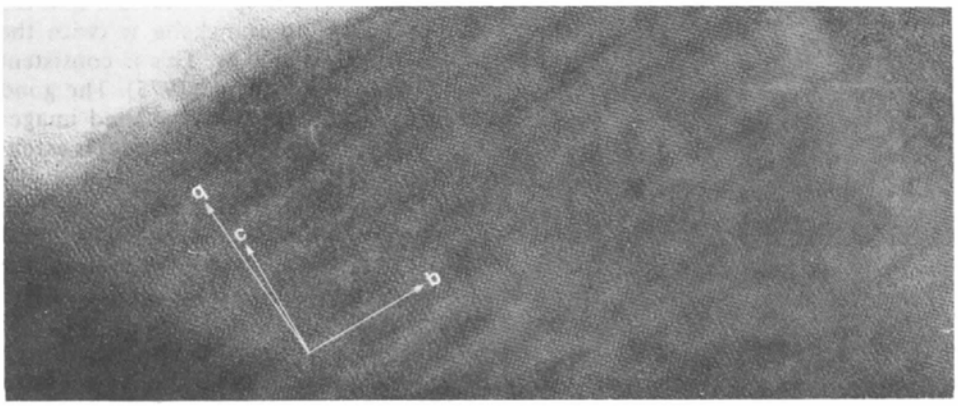

Fig. 8. (100) HRTEM image of franckeite showing that **q** is not parallel to the *c* axis.

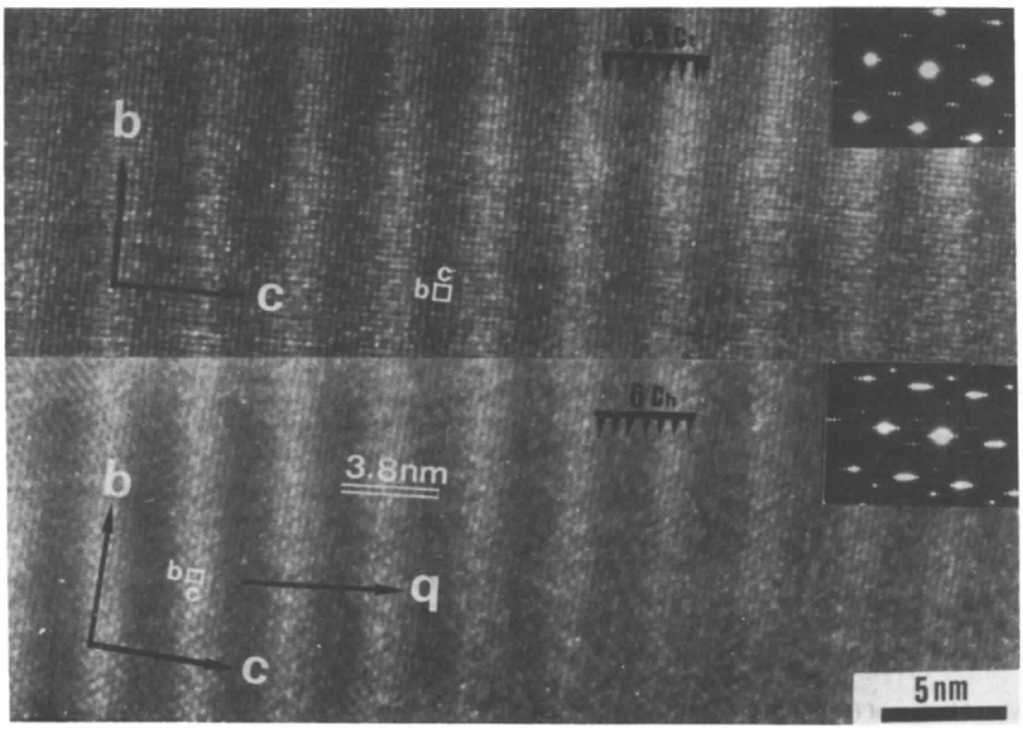

Fig. 9. (100) HRTEM images and the corresponding SAED patterns (insets) of cylindrite showing the modulated wave in the *h* lattice (above) and the *t* lattice (below). The dark bands in the HRTEM images are their common structure modulation.

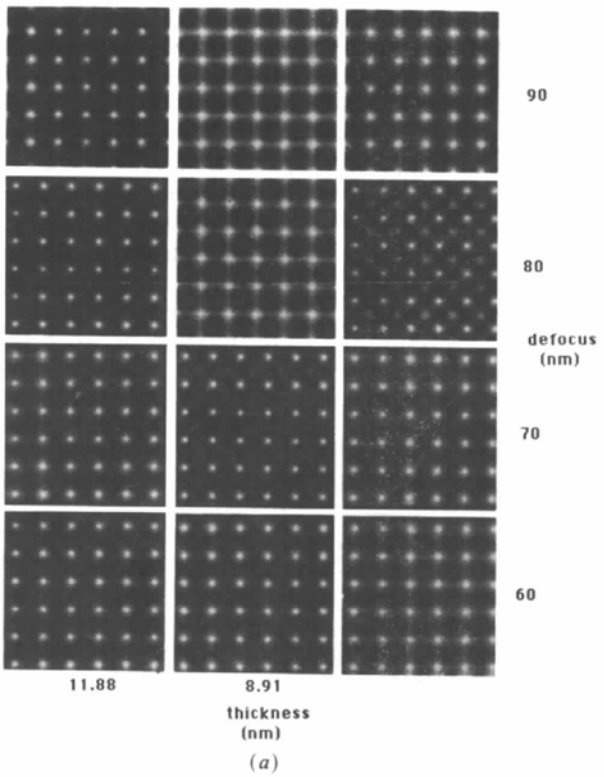

Fig. 10. Simulated images of (100) HRTEM images without considering modulation and sandwich structure. (*a*) Simulated tetragonal lattice image based on PbS structure; (*b*) simulated hexagonal lattice image based on SnS_2 structure.

modulation and the basic axes. Fig. 14 shows the observed and simulated (010) HRTEM images. The observed image is somewhat different from the corresponding image observed by Williams & Hyde (1988*a*, *b*). This may be because the images of Williams & Hyde were recorded slightly off the zone axis. The structure model of franckeite projected on the (010) plane is presented in Fig. 15. The principal difference between the (010) HRTEM images of franckeite and cylindrite is that in cylindrite triple rows of bright spots are separated by dark intervals, whereas in frankeite dark intervals separate quintet rows of bright spots. This phenomenon results from the different compositions of franckeite and cylindrite. The five lines of bright spots indicate that the thickness of the *t* layer in franckeite is twice the thickness of the cylindrite *t* layer. This is consistent with the results of Mozgova *et al.* (1975). The good match between the observed and simulated images in Fig. 14(*b*) shows that this structure model is essentially correct.

Fig. 16 shows the (001) HRTEM image, structure model and corresponding simulated image of franckeite. This simulation does not consider the effects of structure modulation, so the simulated and observed images do not match very well.

In general, the wavelengths of modulation in the structures of franckeite and cylindrite are not constant as demonstrated by the arrows in Fig. 17. Statistically, the wavelength if frackeite is 47 Å and that of cylindrite is 38 Å.

No long-range periodicity has been observed in the *b* direction in either cylindrite or franckeite. It seems that the two layers have no definite matching relation in the *b* direction in these structures.

Discussion

Williams & Hyde (1988*a*, *b*) proved that the step corrugation model of cylindrite was not accurate by comparison of the observed and simulated images based on Makovicky's (1974) model and presented a structure model of cylidrite with sinusoidal corrugation. But some questions, such as how the two types of layers are related to one another and how Sb and Fe are distributed in the structure, need further discussion.

The sinusoidal modulations in these minerals are very similar to those observed in antigorite (Yada, 1979). The structure models of cylindrite and franckeite presented in this paper are based on the structure model proposed by Makovicky (1974) and refined by the alternative wave structure model of Zussman (1954), whose structural principle formed the basis of the crystal structure of antigorite. The models given in the present paper suggest that the Pb atoms are on the surface of the *t* layer and form bonds with S atoms on the surface of the *h* layer resulting

in octahedral coordination. This requires that the two layers match each other. Considering the direction of **q**, if a *t* layer matches an *h* layer, the two layers would have a tendency to curl with the *t* layer on the inner side and the *h* layer on the outer side because the dimensions of the latter are greater than those of the former in that direction. When the *t* layer is on the outer side, the mismatch between the two layers will create dislocations. In this case, the Pb atoms may be substituted by Sb^{3+} atoms and irregular coordination polyhedra will thereby be formed. Similar to the alternating-wave-structure modulation in antigorite, each surface of the *t* layer will alternate on either the outer or the inner side of a curved band. Pb and Sb

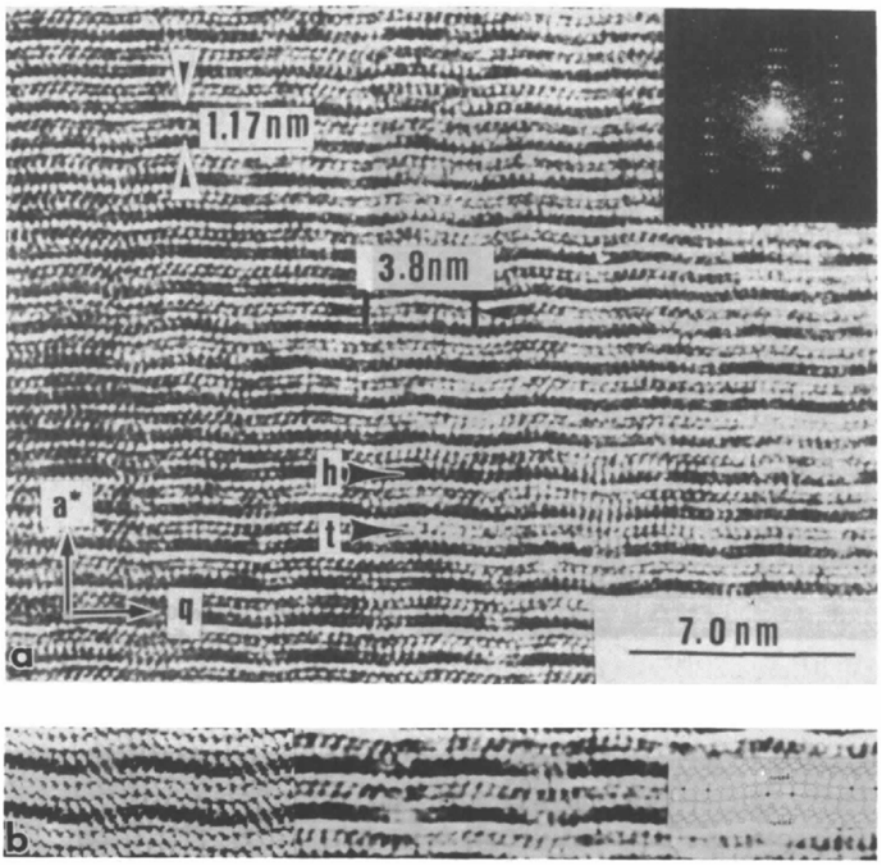

Fig. 11. (010) HRTEM image of cylindrite with its optical diffraction pattern as an inset. (*a*) The sinusoidal modulation wavelength of 38 Å and the stacking periodicity of 11·7 Å, *h* and *t* indicating the *h* layer and *t* layer, respectively; (*b*) comparison of the structure model of cylindrite (right), simulated image based on the model (left) (defocus: 500 Å, thickness: 1200 Å) and observed HRTEM image (center).

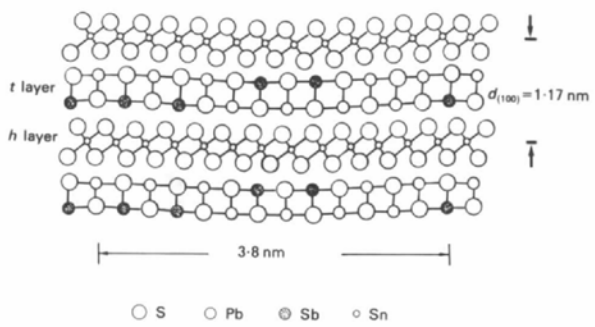

Fig. 12. A structure model of cylindrite projected on (010).

atoms may be distributed alternately on both surfaces of the t layer in the direction of modulation (the direction of $\mathbf{q}$).

If there is only substitution of Pb^{2+} by Sb^{3+} ions, the structure will not be charge balanced. The substitution of Sn^{4+} by Fe^{2+} in the h layer may maintain a charge balance. Therefore, the main cohesive force and the reason for the regular alternating layers are the mutual saturation of opposite excess valencies. The substitutions of Pb^{2+} by Sb^{3+} ions and Sn^{4+} by Fe^{2+} ions are expressed as follows:

$$2Pb^{2+} + Sn^{4+} = 2Sb^{3+} + Fe^{2+}.$$

The atom ratio of Sb to Fe is 2 (Sb : Fe = 2), which is consistent with the ratio in natural and synthetic cylindrite and franckeite (Moh, 1986). Unfortunately, HRTEM images are not sensitive to compositional variation, therefore it is difficult to obtained the exact information necessary to confirm the substitutions. We have suggested possible Sb^{3+} ion positions in the

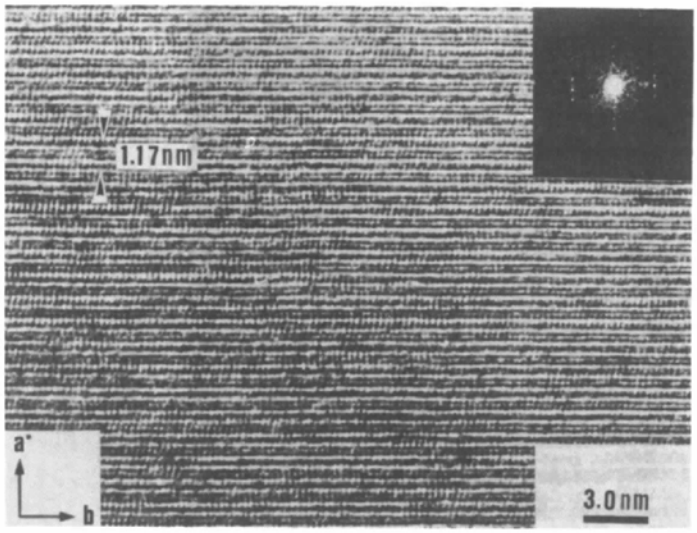

Fig. 13. The (001) HRTEM image of cylindrite with its optical diffraction pattern shown as an inset.

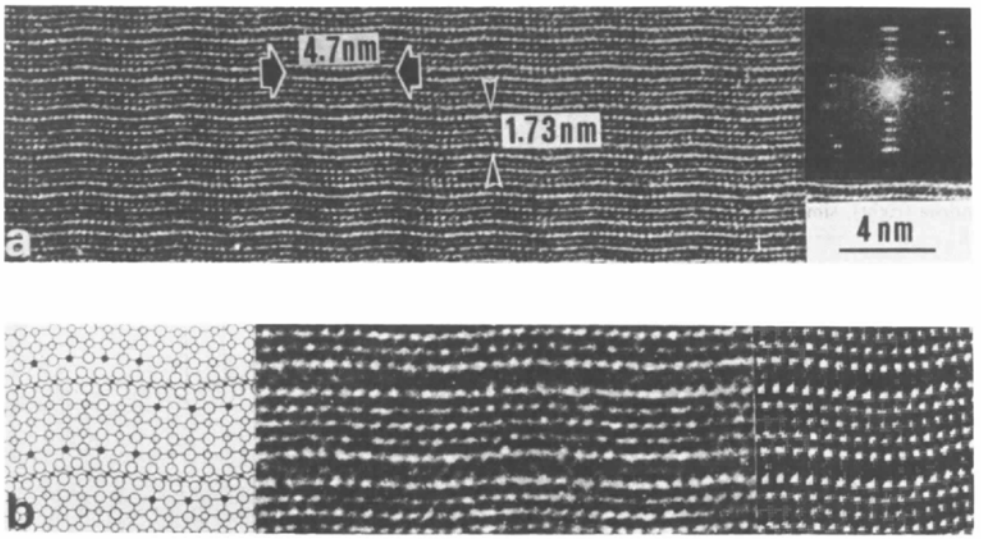

Fig. 14. (010) HRTEM image of franckeite with its optical diffraction pattern as an inset. (*a*) The sinusoidal modulation wavelength of 47 Å and the stacking periodicity of 17·3 Å, h and t indicating the h layer and t layer, respectively; (*b*) comparison of the structure model of franckeite (left), simulated image based on the model (right) (defocus: 550 Å, thickness: 120 Å) and observed HRTEM image (center).

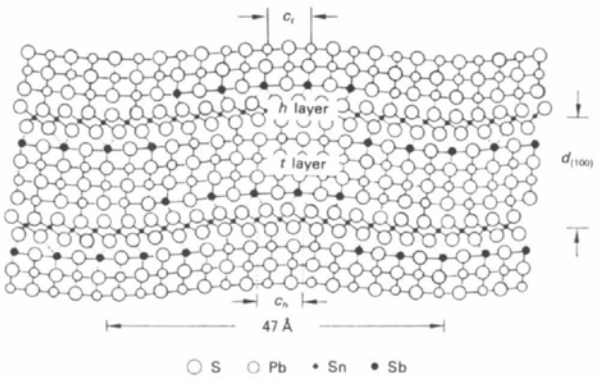

Fig. 15. A structure model of franckeite projected on (010).

models, but have not given possible Fe^{2+} ion positions.

The main difference between the structure of franckeite and cylindrite is the thickness of the *t* layer. The thicker *t* layer of franckeite may be difficult to bend. This may explain why the curvature of the layers in the structure of franckeite is smaller and the wavelength longer than those in cylindrite.

According to the structure model, the composition of the *t* and the *h* layers is [(Pb, Sb)S] and [(Sn, Fe)S_2], respectively. Moh (1986) suggested that there are two types of Sn ion, mainly Sn^{4+} with minor Sn^{2+}, in natural cylindrite and franckeite. The Sn^{2+} ion is in *t* layers and Sn^{4+} ions in *h* layers. Therefore, the composition of the *t* layer would be

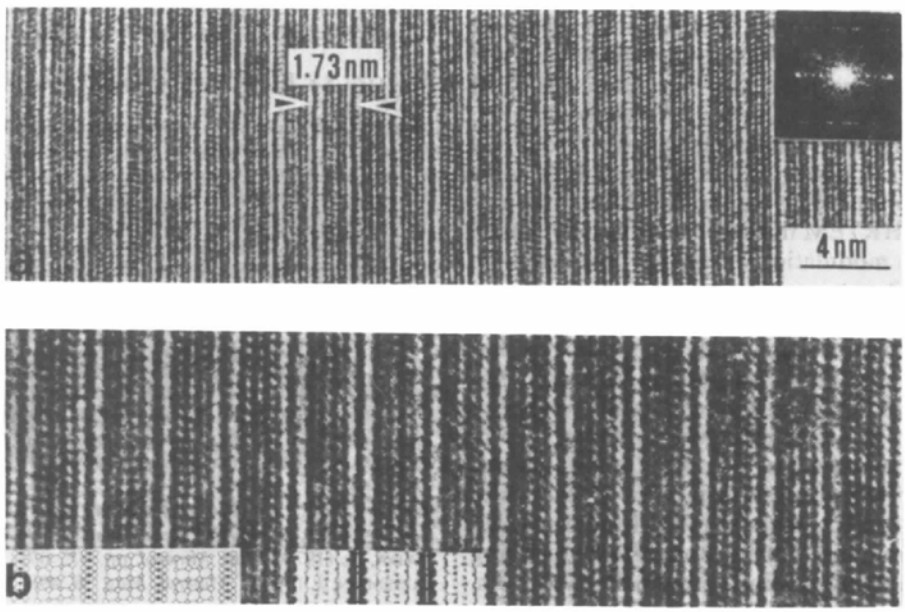

Fig. 16. (*a*) The (001) HRTEM image of franckeite with its optical diffraction pattern inset; (*b*) comparison of the HREM image, structure model (bottom left corner) and simulated image (bottom center, defocus: 550 Å, thickness: 150 Å).

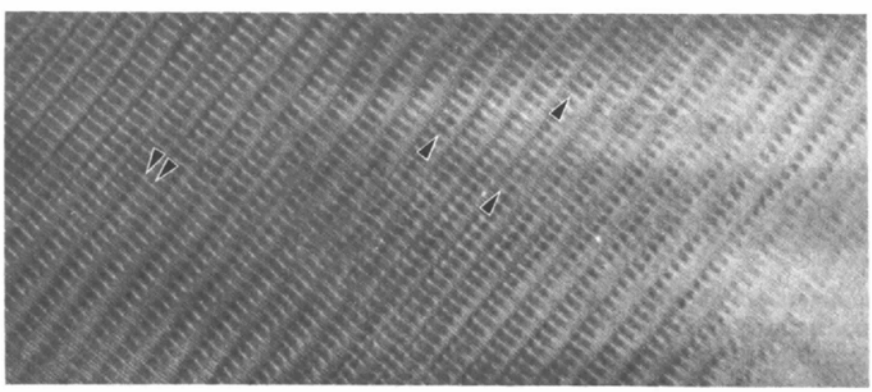

Fig. 17. (010) lattice image of franckeite showing the defects of structure modulation.

[$(Pb, Sb, Sn^{2+})S$] and that of the *h* layer [$(Sn^{4+}, Fe)S_2$]. An approximate common multiple volume (pseudocell) could be determined in both cylindrite and franckeite using the lattice parameters given by Makovicky (1976) and Mozgova *et al.* (1976). The ratio of cations between the two layers in the pseudocells in the models are 2·58 and 1·37 for franckeite and cylindrite, respectively. Following Evans & Allmann (1968), we can express the crystallochemical formulae of franckeite and cylindrite as follows:

franckeite $2{\cdot}58[(Pb^{2+}, Sb^{3+}, Sn^{2+})S][(Sn^{4+}, Fe^{2+})S_2]$

cylindrite $1{\cdot}37[(Pb^{2+}, Sb^{3+}, Sn^{2+})S][(Sn^{4+}, Fe^{2+})S_2]$.

Concluding remarks

Makovicky (1976) and Williams & Hyde (1988*a*, *b*) previously presented b^*c^* transmission electron diffraction patterns of cylindrite and Williams & Hyde (1988*a*, *b*) also presented corresponding HRTEM images. Our results are somewhat different from these. The present TEM study indicates that the two layers in cylindrite have different stacking vectors. In addition, separate *h*- and *t*-layer electron diffraction patterns and their HRTEM images were obtained. Based on the common modulation of the two layers and the common CBED patterns, the relations between the two lattices and between the lattices and the modulations were determined. This study also indicates that there are two types of incommensurability in cylindrite and franckeite, the incommensurability between the two lattices in each structure and the incommensurability between the lattices and modulations. The alternative wave-structure models of cylindrite and franckeite are suggested, simulated and discussed in this paper, pointing out the modulations resulting from the mismatching relation between the two layers.

The authors thank Professors E. M. Huang and Z. S. Ma for providing the cylindrite and franckeite samples for this study. Discussions with Professors Y. M. Chu, K. K. Feng and F. H. Li are gratefully appreciated.

References

AALST, W. VAN, DEN HOLLANDER, J., PETERSE, W. J. A. M. & DE WOLFF, P. M. (1976) *Acta Cryst.* **B32**, 47-58.

EVANS, H. T. & ALLMANN, R. (1968). *Z. Kristallogr.* **127**, 73-79.

FRENZEL, A. (1893). *Neues Jahb. Mineral Geol. Palaeontol.* **2**, 125-128.

HIRSCH, P. B., HOWIE, A., NICHOLSON, R. B., PASHLEY, D. W. & WHELAN, M. J. (1977). *Electron Microscopy of Thin Crystals.* New York: Kireger.

HUANG, M., WU, G., CHEN, Y. & TANG, S. (1986). *Acta Geol. Sin.* **2**, 164-175.

JANNER, A. & JANSSEN, T. (1977). *Phys. Rev. B*, **15**, 643-658.

JANNER, A. & JANSSEN, T. (1980). *Acta Cryst.* **A36**, 399-408, 408-415.

KISSIN, S. A. & OWEUS, D. R. (1986). *Can. Mineral.* **24**, 45-50.

MAKOVICKY, E. (1971). *Neues Jahb. Mineral. Monatsh.* pp. 404-413.

MAKOVICKY, E. (1974). *Neues Jahrb. Mineral. Monatsh.* pp. 235-256.

MAKOVICKY, E. (1976). *Neues Jahrb. Mineral. Abh.* **126**, 304-306.

MOH, G. H. (1984). *Mineral. Abh.* **150**, 25-64.

MOH, G. H. (1986). *Neues Jahrb. Mineral. Abh.* **153**, 267-272.

MORITZ, H. (1933). *Neues Jahrb. Mineral. Beil.* **66**, Abt. A, 191-212.

MOZGOVA, N. N., BORODAYEV, YU. S. & SVESHNIKOVA, O. L. (1975). *Dokl. Akad. Nauk SSSR*, **220**, 107-110.

MOZGOVA, N. N., ORGANOVA, N. I. & GORSHKOV, A. I. (1976). *Dokl. Akad. Nauk SSSR* (*Engl. transl.*) **228**, 110-113.

RAMDOHR, P. (1960). *Die Erzmineralien und ihre Verwachanngen.* Berlin: Akademie Verlag.

WANG, S. (1988). *Inst. Phys. Conf. Ser.* No. 93, Vol. 2, p. 331.

WANG, S. (1989). *47th Annual Proc. Electron Microscopy Soc. of America*, edited by G. W. BAILEY, p. 420. San Francisco Press.

WILLIAMS, T. B. & HYDE, B. G. (1988*a*). *Acta Cryst.* **B44**, 467-474.

WILLIAMS, T. B. & HYDE, B. G. (1988*b*). *Phys. Chem. Miner.* **15**, 521-544.

WOLFF, P. M. DE (1974). *Acta Cryst.* **A30**, 777—785.

WOLFF, P. M. DE (1977). *Acta Cryst.* **A33**, 493-497.

YADA, K. (1979). *Can. Mineral.* pp. 679-691.

ZUSSMAN, J. (1954). *Mineral. Mag.* **30**, 498.

Acta Cryst. (1991). A47, 392-400

Accurate Bond and Angle Parameters for X-ray Protein Structure Refinement

BY RICHARD A. ENGH AND ROBERT HUBER

Max Planck Institut für Biochemie, D8033 Martinsried bei München, Germany

(*Received* 14 *November* 1990; *accepted* 17 *January* 1991)

Abstract

Bond-length and bond-angle parameters are derived from a statistical survey of X-ray structures of small compounds from the Cambridge Structural Database. The side chains of the common amino acids and the polypeptide backbone were represented by appropriate chemical fragments taken from the Database. Average bond lengths and bond angles are determined from the resulting samples and the sample standard deviations provide information regarding the expected variability of the average values which

0108-7673/91/040392-09$03.00